Fuel 407 (2026) 137561

Contents lists available at ScienceDirect

Fuel

journal homepage: www.elsevier.com/locate/fuel

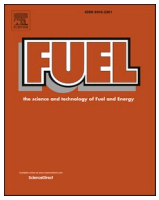

Full Length Article

Thermal cracking of polyolefin waste: Primary and secondary product formation as a function of gas phase residence time in bubbling fluidized bed

Surika van Wyk *, Carlos F. Mourao Vilela, Carel Meijwes, Marco Geusebroek, Arnold Toonen

Biobased and Circular Technology Group, Energy & Materials Transition unit, The Netherlands Organization for Applied Scientific Research (TNO), Petten, the Netherlands

ARTICLE INFO

Keywords:
Residence time
Thermal cracking
Fluidized bed
Waste
Olefins
Secondary reactions

ABSTRACT

The effect of gas phase residence time on the product slate during the thermal cracking of polyolefins was experimentally investigated in a bubbling fluidized bed reactor at a temperature of 750 °C and a steam-to-carbon ratio of 0.8. Three feedstocks were investigated: polyethylene (PE), polypropylene (PP) and a real-world sorted waste stream (DKR-350). Product gases were simultaneously measured at three different heights above the fluidized bed, corresponding to residence times of 1.6–10 s. All feedstocks yielded a product gas rich in CH_4, C_2H_4 and C_3H_6. The increasing yield of CH_4 and H_2 with residence time indicated the progression of secondary reactions, as the primary products decreased. C_3H_6 was the most reactive primary product, with yields decreasing significantly (37–47 % within three seconds) with residence time, whereas the C_2H_4 yield remained relatively stable. The higher C_3H_6 reactivity was related to reduced thermal stability, caused by the additional methyl group. For the aromatics, the benzene yields increased notably, due to the cyclization reactions of C_3H_6. The largest effect of residence time was seen from 1.6 to 5 s, after which the effect decreased due to a reduction in the free radicals concentration which promotes secondary reactions via different pathways, including radical propagation and recombination. The results demonstrated the role of gas phase residence time in the formation of secondary products during thermal cracking of polyolefins. The findings assist with process optimization towards target components, by adjusting the residence time and controlling the occurrence of secondary reactions.

1. Introduction

Plastic waste is a continuous global challenge with waste production increasing daily with the growth of global population and increased consumerism. In 2019, the global waste production was 353 Mt and is projected to increase to 833–874 Mt by 2050 [1,2]. The detrimental effect of plastic waste is well known, contributing to pollution (air, soil and water), loss of biodiversity and posing health risks to humans [1,3–5]. Plastics are mainly fossil-based (> 90 %), with less than 10 % originating from circular sources, primarily through mechanical recycling of post-consumer waste [6]. Plastic waste has a high carbon content, making it a valuable source of carbon and a potential feedstock that could be leveraged for the production of new plastics. Utilizing plastic waste as a feedstock reduces the dependence on fossil fuels, while addressing the plastic waste management challenges, thereby advancing the transition towards a more circular economy [7–9]. Despite efforts to collect and sort plastic waste for recycling, the majority is still landfilled or incinerated, resulting in carbon loss and CO_2 emissions [10]. Only 9 % of the global plastic waste was actually recycled in 2019 [2].

One of the main challenges of recycling plastic waste is its heterogeneous nature due to the numerous polymers used in the production of different plastics, contaminants (from fillers and additives) and the biogenic fraction resulting from paper, food residues and textiles [3,9,11]. Mixed plastics waste (MPW) largely originates from post-consumer packaging and products, and consists mainly of polyolefins (~75 %) including polypropylene (PP) and polyethylene (PE), with smaller fractions of polystyrene (PS), poly vinyl chloride (PVC) and polyethylene terephthalate (PET) [9]. Mechanical and chemical recycling methods require cleaner homogenous streams, and the available capacity of these processes is not able to meet the large volume of plastic waste generated. Moreover, these plastic streams can only be

* Corresponding author.
E-mail address: surika.vanwyk@tno.nl (S. van Wyk).

https://doi.org/10.1016/j.fuel.2025.137561
Received 11 September 2025; Received in revised form 28 October 2025; Accepted 14 November 2025
Available online 20 November 2025

Nomenclature

ar	As received
BFB	Bubbling fluidized bed
BT	Bed temperature
BTXS	Benzene, toluene, xylene and styrene
C–C	Carbon-Carbon
C–H	Carbon-Hydrogen
daf	Dry, ash-free basis
db	Dry basis
GC	Gas-chromatographer
FBT	Freeboard temperature
FID	Flame ionisation detector
IPA	Isopropanol
MPW	Mixed plastic waste
PA	Polyamide
PAH	Polycyclic aromatic hydrocarbons
PE	Polyethylene
PET	Polyethylene terephthalate
PP	Polypropylene
PS	Polystyrene
PVC	Polyvinyl chloride
SI	Supporting Information
StC	Steam-to-carbon
WGS	Water-gas-shift

mechanically recycled a finite number of times before the polymer chains become too degraded, where further recycling is no longer feasible, resulting in the stream being either landfilled or incinerated [5,8,12,13].

Thermochemical conversion processes such as gasification, pyrolysis and thermal cracking are mature technologies and offer solutions for treating larger volumes of heterogeneous plastic waste streams [3,8,9,12,14,15]. Thermal cracking (also referred to as thermal pyrolysis or steam cracking) is a process which involves the direct recovery of monomers via thermal decomposition of plastic waste. The process operates in the presence of steam at temperatures ranging from 700–900 °C, producing a monomer-rich product gas. Unlike steam gasification (which yields syngas) and traditional pyrolysis (which produces plastic oil for steam crackers), thermal cracking targets monomers [7,16]. For the polyolefin-rich MPW streams, the resulting product gas is rich in olefins, similar to the traditional steam crackers of naphtha and other fossil fuel feedstocks. The recovered monomers can be used for the production of virgin quality plastics, by integrating this system at the back end of a conventional steam cracker [3]. With this method carbon sources traditionally derived from fossil fuels are replaced with plastic waste, thereby reducing fossil fuel dependence, lowering CO_2 emissions (less incineration) and contributing to more effective plastic waste management. This technology is also capable of processing large volumes of plastic waste by leveraging existing petrochemical infrastructure, making it scalable and industrially viable [3,7].

To optimize the light olefins yield, secondary reactions are avoided/minimized by controlling parameters such as temperature, residence time and flow rate. Secondary reactions occur when the primary cracking products react further to produce secondary products, which in the case of steam cracking consists of aromatics, H_2, CH_4 and solid carbon (soot) [17–19]. Analogous with steam cracking, the operating parameters for thermal cracking of plastic waste for light olefins recovery must be carefully optimized to minimize secondary reactions and maximize the light olefins yield. Temperature and residence time are the two main parameters affecting the occurrence of secondary reactions, with higher temperatures and longer residence times promoting secondary reactions [9,11,14]. For conventional steam cracking, it was shown that the residence time and temperature profiles within the reactors were strongly correlated. The cracking severity is expressed as a function of the both parameters, with a stronger dependence on the temperature than on the residence time [19,20]. For thermal cracking of plastic waste, numerous studies have investigated the effect of temperature on the product distribution of various plastics, however studies on the effect of residence time are limited and only focussed on testing monomer streams (PE and PP) under pure pyrolysis conditions (pure N_2 atmosphere) rather than real post-consumer plastic waste [21–27]. Shah et al. [27] reviewed the effect of residence time for different plastic pyrolysis studies and stated that both residence time and pressure are temperature-dependent variables (similar to conventional steam cracking), with the effect of residence time becoming less evident at higher temperatures. Nevertheless, to advance the development of this technology for the recycling of MPW, it is important to understand the role of residence time on the product distribution, to ensure optimization of the parameters for target products [9,15].

Mastral et al. [26] and Jung et al. [21] studied the effect of residence time of PE and PP in a fluidized bed, by adjusting the flow rates of N_2 in the reactor. The drawback of this method is that if the feed rate is kept constant the product gas becomes diluted, which will also affect secondary reactions (more dilution, less secondary reactions). At the same time, the hydrodynamics in the reactor change and the measurement accuracy of the instruments can also vary with the different concentrations. Natesakhawat et al. [25] and Westerhout et al. [23] studied the effect of residence time on PE and PP, by adapting the experimental set-up i.e. smaller tube diameter and changing the position of the sampling probe. This method avoids adjusting the flow rate, however, the reactor modifications can still affect the hydrodynamics. The experimental variability from repeated tests is inherently coupled with the effect of residence time, making it difficult to isolate the effect of residence time especially when measurement errors are large and influence of residence time is minimal.

The aim of this study was to investigate the role of gas phase residence time on the thermal cracking of polyolefins. Pure PP and PE were investigated together with a real polyolefin-rich sorted plastic waste stream namely DKR-350. The product gas was simultaneously measured at different locations in the reactor, to enable the direct comparison of the effect of gas phase residence time on the product distribution of plastic thermal cracking, eliminating the effect of inconsistent hydrodynamics, experimental variability and dilution effects. The product distribution of gas phase components, as well as the aromatics were compared for different gas phase residence times to quantify the extent of secondary reactions. The results provide insight into the effect of gas phase residence time on the product distribution of MPW thermal cracking, which will aid reactor design and parameters optimization for targeted product distributions.

2. Experimental set-up

2.1. Materials

Two pure polymers, namely PE and PP were investigated together with a real mixed plastic waste stream namely DKR-350, with a PE-PP content of circa 68 % (dry basis). The composition of the DKR-350 stream was determined by sorting, characterization and washing, with a detailed description of a similar characterization method given in [28]. The PE-to-PP ratio was 2:1. The remaining fractions consisted of other plastics such as PET, PS, polyamide (PA) etc., as well as a biogenic fraction from paper and food residue. The PE and PP were in the form of circa 3 mm beads. The PE (high density PE) was Marlex PE supplied by

Chevron Philips Chemical Company. The PP was supplied by Borealis. The DKR-350 feedstock was provided by a Dutch industrial waste sorter and the feedstock preparation was done in-house. The feedstock preparation included shredding, pelletisation and milling of the pellets to produce circa 6 mm particles suitable for feeding to the laboratory-scale reactor via the screw feeding system. The DKR-350 particles were larger than the pure PE and PP beads, however the density was lower. In Fig. S1, in the supporting information (SI), the feedstocks are compared. In this study, only the gas phase residence time above the fluidized bed was evaluated using the top of the bed as the baseline (see Section 2.3). The assumption was made that the feedstock was fully devolatilized at this point. Representative samples were taken of each feedstock and sent for proximate and elemental analysis along with calorific value. The results are presented in Table 1.

2.2. Experimental set-up

In Fig. 1 the schematic of the multi-purpose bubbling fluidized bed (BFB) reactor with the accompanying gas analysis trains is given. The installation is located at the TNO site in Petten, the Netherlands.

The reactor was divided into two zones, the bottom zone (where the bed is located), with an inner diameter and height of 74 and 500 mm respectively. The second zone, is the freeboard with an inner diameter and height of 102 and 600 mm respectively. The reactor was operated under atmospheric pressure and supplied with heating elements at the wall to provide external electrical heating. Solid feedstock was fed via a calibrated screw feeder (maximum capacity of 500 g/h) directly into the hot fluidized bed at the bottom of the reactor. The feeding screw was equipped with external cooling to ensure that the plastics did not melt in the feeding screw before entering the bed. The feeding bunker was weighed before and after each test to determine the average feeding rate over the experimental time, which was taken as the feed rate for the calculations (see Section 2.4). The reactor was equipped with numerous K-type thermocouples at various locations along the reactor (see Fig. 1) to monitor the temperature profiles and ensure even temperature distribution during experiments. In the SI, the temperature profiles are provided as examples. Pressure sensors were located at multiple locations within the rector to monitor the internal pressure and pressure drops and assess the fluidization behaviour of the bed.

For each experiment, the reactor was filled with 1.3 kg of quartz sand (dp50 = 310 μm; Dorsilit® 9 Cristal quartz sand (94 % SiO_2) supplied by Dorfner). The static bed height was 112 mm and the fluidized bed height was estimated to be 195 ± 5 mm. Steam was used as fluidization medium (pre-heated to 200 °C), and the flow rate was set so that the steam-to-carbon (StC) ratio was 0.8 g/g. Nitrogen (N_2) was added as additional fluidization medium (along with steam), so that the total flow (product gas including tars) was ± 2.5 times the minimum fluidization velocity. This ensures consistent hydrodynamics and equal flow rates across tests, enabling comparable residence times. Neon (Ne) was added to the bottom of the reactor (20 NmL/min) as a tracer gas to determine the volumetric flow of the product gas. The temperature was set to 750 °C for all three feedstocks. One experiment was also performed at 700 °C for the PE feedstock. The results of the experiment at 700 °C were only used for the comparison of the cracking severity coefficient (see Section 3.4) to compare the effect of temperature and gas phase residence time. The experimental conditions are summarized in Table 2.

The temperatures of the tracing were measured directly on the outside of the wall close to the tracing elements, below the insulation material. The process values of the tracing sections above the fluidized bed (tracing 2 and 3) were lower than the measured gas phase temperatures, as the set points were lower to ensure that gas phase temperature remained constant. The lower values also assisted with mitigating the occurrence of secondary reactions associated with higher wall temperatures. For the bottom section, where the bed was located, the tracing temperature was equal to the measured temperatures inside the bed.

Table 1
Feedstock analysis results.

		PE	PP	DKR-350
Calorific value	MJ/kg (db)[a]	44.0	46.2	35.7
Proximate analysis				
Ash (at 550 °C)	wt.% (db)	< 0.1	< 0.1	8.5
Moisture	wt.% (ar)[b]	< 0.1	< 0.1	1.5
Volatiles	wt.% (db)	99.9	99.9	88.3
Elemental analysis				
C	wt.% (db)	85.7	85.7	70.1
H	wt.% (db)	14.3	14.3	11.0
N	wt.% (db)	0	0	0.6
O[c]	wt.% (db)	0	0	9.7
S	wt.% (db)	0	0	0.14
Br	mg/kg (db)	0	0	8.8
Cl	mg/kg (db)	0	0	3,843
F	mg/kg (db)	0	0	47.6

[a] db – dry basis.
[b] ar – as received basis.
[c] Directly measured (not calculated by difference).

2.3. Analysis and gas phase residence time calculations

To measure the effect of gas phase residence time on the product gas composition, the product gas was measured simultaneously (online and offline) at three different locations inside the reactor, as shown in Fig. 1. The first measurement point (A) was located above the fluidized bed (455 mm above the bed plate (indicated by the dashed line in Fig. 1)). The second measurement point (B) was located in the middle of the freeboard (740 mm above the bed plate) and the last point (C) was located at the exit of the reactor (1100 mm above the bed plate). Each analysis point was equipped with a filter and tar sampling train which served as a pre-sampling system to prevent solids, moisture and tar (defined as polycyclic aromatic hydrocarbons (PAHs) with a molecular weight greater than toluene) from entering the gas analysers. The sampling line up to the filter and the filter itself were heated to 450 °C (via electrical tracing) to avoid condensation of tar in the lines. The temperature of the sampling lines was well below the experimental operating temperature (see Table 2), to ensure that no secondary reactions would occur in the sampling line. After the filter, impinger bottles filled with isopropanol (IPA) solution were placed to capture the tar components, as well as benzene and toluene, from the product gas (done according to the wet chemical sampling for the standardised tar measurement protocol [29]). This served as both the pre-sampling system to protect the online analysers, and to sample and quantify the tar components as well as benzene and toluene. The run time for each experiment was circa three hours and the flow rate of the sampled gas was set to 0.5 NL/min (as opposed to the 3 NL/min according to the standardised tar measurement protocol [29]). The flow rate was lower and the run time was fixed to ensure that the IPA solution did not become oversaturated with aromatics, leading to a concentration breakthrough. The lower sampling rate also minimizes the effect of product gas sampling on the gas phase residence time, as higher sampling rates lower the product gas flow and consequently increases the residence time. The analysers at the end of each train measured benzene and toluene and the concentrations were monitored to ensure that no breakthrough occurred. The composition of the dry, tar-free product gas was measured using online analysers and micro or compact gas-chromatographer (GC) analysers (relative error 2–5 %). Offline analysis was performed by sampling the product gas via gas bags and directly analysing the samples with a Thermo Scientific Trace 1310 GC with flame ionisation detector (GC-FID), to quantify the C_1–C_6 hydrocarbons and H_2. In Table 3, the analysis and analysers are summarised. In Table S1 (SI), further details of the analytical equipment are provided as well as in [30].

To correct for the minor differences in concentration between the

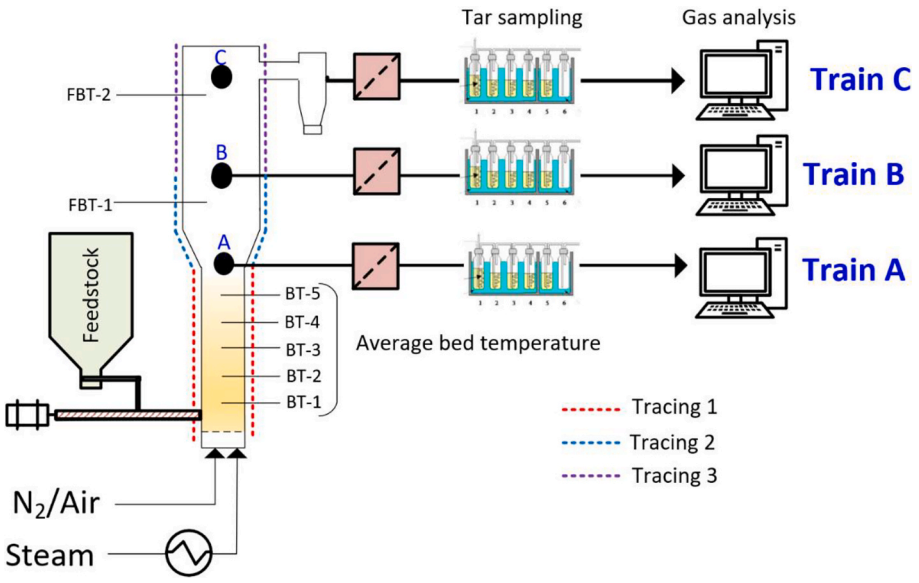

Fig. 1. Schematics of the bubbling fluidized bed installation with modified analysis trains and thermocouple locations (BT – bed temperature; FBT – freeboard temperature).

Table 2
Measured experimental conditions for each test.

Parameter	Unit	Run 1	Run 2	Run 3	Run 4
Feedstock	-	PE	PP	DKR-350	PE
Duration of run	min	185	193	197	188
Process value of Tracing 1	°C	750 ± 1[h]	745 ± 3[h]	751 ± 3[h]	700[i]
Process value of Tracing 2	°C	733 ± 3[h]	729 ± 3[h]	732 ± 3[h]	700[i]
Process value of Tracing 3	°C	731 ± 3[h]	727 ± 3[h]	728 ± 2[h]	700[i]
Average bed temperature[a] (point A)	°C	742 ± 4[g]	737 ± 3[g]	744 ± 3[g]	692.6 ± 4[g]
Temperature above the bed[b] (point B)	°C	744 ± 3[h]	740 ± 3[h]	744 ± 3[h]	694 ± 2[h]
Freeboard temperature[c] (point C)	°C	746 ± 3[h]	742 ± 3[h]	744 ± 2[h]	694.1 ± 0.1[h]
Feeding rate	g/h (ar)[d]	206	184	209	206
N_2 flow[e]	NL/min	7.0	8.0	9.0	7.0
Steam flow	g/h	136	137	107	136
Steam/Carbon ratio[f]	g/g	0.77	0.74	0.74	0.77
Total velocity of steam + N_2 in bed[j]	m/s	0.14	0.15	0.16	0.13

[a] Average of the five bed temperatures measured (average of BT-1 to BT-5 in Fig. 1).
[b] Temperature reading of FBT-1 (see Fig. 1).
[c] Temperature reading of FBT-2 (see Fig. 1).
[d] On as received (ar) basis.
[e] Including the 1 NL/min N_2 on the feeding screw.
[f] Includes the moisture of the feedstock.
[g] Standard deviation between five measurements in the bed.
[h] Standard deviation of the measurement itself.
[i] Set point values, process values were not recorded.
[j] Minimum fluidization velocity is 0.068 m/s.

Table 3
Summary of the product gas analysis for the experiments.

Components	Location	Sampling	Analyser
CO, CO_2, CH_4, H_2 and O_2	A, B and C	Online	ABB gas analyser (used for monitoring product gas composition during experimental run) Quantification of solids carbon in the bed
N_2, Ne, Ar/O_2, CO, CO_2, CH_4, C_2H_2, C_2H_4, C_2H_6, benzene, toluene H_2S and COS	A	Online	Varian micro-gas chromatographer (GC) analyser. Quantification of CO and CO_2 and product gas flow rate
N_2, Ne, Ar/O_2, CO, CO_2, CH_4, C_2H_2, C_2H_4, C_2H_6, C_3H_6, C_3H_8, benzene, toluene H_2S and COS	B	Online	Varian micro-gas GC analyser. Quantification of CO and CO_2 and product gas flow rate
N_2, H_2, Ne, Ar/O_2, CO, CO_2, CH_4, C_2H_2, C_2H_4, C_2H_6, C_3H_6, C_3H_8, benzene, toluene H_2S and COS	C	Online	Compact-GC analyser. Quantification of CO and CO_2 and product gas flow rate
C_1-C_6 hydrocarbons and H_2	A, B and C	Offline gas bag	Thermo Scientific Trace 1310 GC with a flame ionisation detector (GC-FID). Quantification of C_1-C_6 hydrocarbons and H_2
Benzene, toluene and PAHs	A, B and C	Offline tar guideline sampling	GC-FID. Quantification of benzene and toluene and PAHs.

online analysers (micro-GC's and compact-GC), the concentration of components was compared for the analysers by simultaneously measuring at the same exact analysis point. In this manner the influence of different analysers could be assessed and decoupled from the difference in product gas composition due to residence time. The difference between the analysers was < 0.4 vol% (average 0.2 vol%) for both CO and CO_2. Note this is only applicable to the CO, CO_2 and tracer concentrations. The product gas flow rate at points A and B was corrected using the Ne ratio obtained from offline GC-FID analysis. The compact-GC provided the most accurate quantification of the product gas flow (Ne measurements) and the gas flow rate at point A and B was corrected accordingly as shown in Eq. (1).

$$\dot{Q}_i = \frac{\dot{Q}_{i,GC-FID}}{\dot{Q}_{C,GC-FID}} \times \dot{Q}_{C,compact-GC} i = A, B \quad (1)$$

where $\dot{Q}$ is the volumetric flow rate (Nm^3/s) at point *i*. For the other non-condensable components, the quantification was done by taking gas

bags simultaneously during steady state operations and analysing the gas bags on the same GC-FID analyser. The IPA solutions were also all analysed using the same equipment.

For the gas phase residence time, the baseline was taken at the top of the fluidized bed (195 mm) and the gas phase residence time for point A, B and C was calculated based on the volume and volumetric product flow rate determined at each point, see Eq. (2).

$$\tau_i = \frac{V}{\dot{Q}_i} i = A, B, C \tag{2}$$

where τ_i is the approximated average residence time of the gas (in seconds) at either point A, B or C, $\dot{Q}_i$ is the volumetric flow rate (m^3/s) at point A, B and C (corrected for the sampling rate), and V is the volume of the reactor (m^3) from the baseline to point A, B or C respectively. Eq. (2) assumes an ideal plug flow regime in the freeboard, neglecting the effect of axial dispersion. Prior to the tests a pulse test was performed by injecting CO_2 as a tracer at the bottom of the reactor and measuring the concentration responses at different points. Analysis of the cumulative residence time distribution curves and the approximated dispersion number indicated moderate deviations from ideal plug flow in the freeboard. Moderate axial dispersion in the freeboard could affect the concentration profiles and the difference in the measured concentrations would not be due to residence time alone, but also due to hydrodynamic effects such as back-mixing. The axial dispersion is however moderate and the effect of residence time is considered as the dominating effect. Variations in the gas concentrations are accounted for in the error propagation calculations.

2.4. Product yield and cracking severity

After each experiment, when the feeding rate was stopped, air was introduced to the bottom of the bed to combust the residual carbon in the bed. The CO_2 (and CO) concentrations were measured and used to quantify the solid carbon for each experimental run. For the gas phase products, the yield of each component was calculated according to Eq. (3):

$$n_i = \left(\frac{c_i \times \dot{Q}}{22.414}\right) \times \frac{1}{\dot{m}_{Feedstock(daf)}} \tag{3}$$

In Eq. (3), n_i denotes the molar yield of component i in mol/kg. c_i is the volume concentration (vol.%) of species i and $\dot{Q}$ the volumetric flow rate (NL/h) at the respective sampling points. $\dot{m}$ is the mass flow rate of the feedstock (kg/h) on a dry-ash free (daf) basis. Multiplying the value with the molecular weight of the species i gives the mass yield in g/kg, which was used for the aromatics. For the carbon yields the calculation was as follow, Eq. (4).

$$\%C_i = \left(\frac{n_i}{nC_{total}}\right) \times x_{carbon,i} \times 100 \tag{4}$$

where $\%C_i$ is the carbon yield of species i, nC_{total} is the total moles of carbon in 1 kg of feedstock and $x_{carbon,i}$ is the fraction of carbon in molecule i. With the carbon yields, the total carbon balance for each run was calculated. Errors in product yields and mass balance closures were quantified using the error propagation method, with further details provided in the SI. The cracking severity was calculated to evaluate the effect of gas phase residence time. The cracking severity coefficient proposed by Mandviwala et al. [31] was adopted for this study and was calculated according to Eq. (5). The lower the cracking severity, the higher the cracking severity coefficient (−) as it is inversely proportional to CH_4, which will increase with secondary reactions.

$$Crackingseveritycoefficient = \frac{n_{C_2H_4} + n_{C_3H_6} + n_{C_4H_8}}{n_{CH_4}} \tag{5}$$

3. Results and discussion

3.1. Overall product distribution

The mass yields of the non-condensable gas, aromatics and solids for the different feedstocks and gas phase residence times are compared in Fig. 2 for a temperature of 750 °C. The carbon yields were also calculated and can be found in the SI.

The mass yields were not normalized and the expected mass balance closure is 100 ± 10 % accounting for errors in analysis, sampling and feeding. For PP (point A), the mass balance closure was lower, than the expected ± 10 % deviation. The larger deviation was due to an underestimation of the product flow rate, as the sum of the volume concentrations were ± 100 vol.% and the same feeding rate was used for all three points, with B and C having a balance closure within 10 %. With a higher product flow rate, the mass yields of all the components (except the solids carbon) would increase, leading to an overall increase in mass balance closure. Despite the lower yields, the trends in the product gas concentrations (independent of flow rates) were consistent with the yield trends reported in this and subsequent sections (see the SI, Fig. S7 toS9 for the concentration comparisons of PP).

In general, the majority of the mass in the feedstock (55 – 70 m/m%, depending on feedstock and sampling position) goes to the non-condensable product gas which includes the hydrocarbons C_1–C_6, CO and CO_2 concentrations. The yields of the condensable products namely benzene + toluene and other aromatics were comparable, with the benzene + toluene having a slightly higher yield (13–20 m/m%). The solid residue has the lowest yield of all the products, given the high volatile content of the feedstocks (88–99 wt%) and consequently the low fixed carbon content. For pure PP and PE, the yields were 2 m/m%, which is mainly due to the soot formation as the volatile content was 99.9 wt% (see Table 1). For DKR-350, the yield of solid residue was higher (3.4 m/m%) due to the formation of soot as well as some char formed from the biogenic fractions of the feedstock.

The reported mass yields were comparable with yields reported in previous studies for pure PP and PE pyrolysis and thermal cracking. In Table 4, the main products mass yields are reported and compared.

Product gas yield reported by Mandviwala et al. [31] were higher

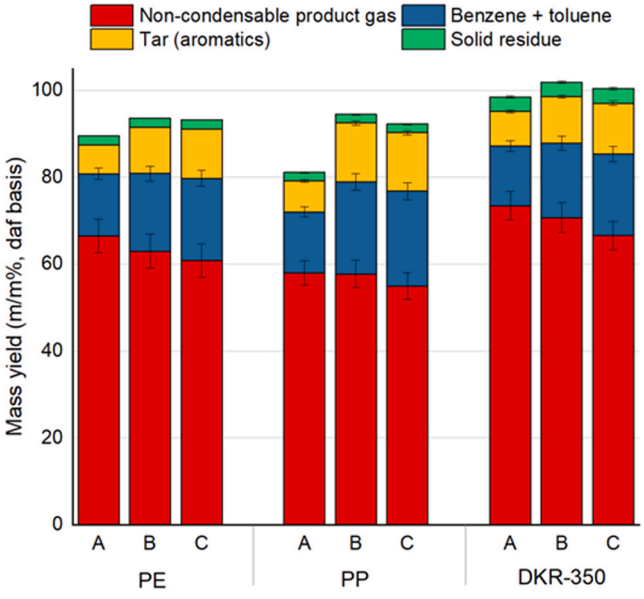

Fig. 2. Comparison of the product distribution for the different feedstocks at different residence times at 750 °C (PE: A = 1.8 s; B = 5.1 s, C = 9.7 s/ PP: A = 1.6 s; B = 4.4 s, C = 8.2 s / DKR 350: A = 1.6 s; B = 4.6 s; C = 8.6 s; Error bars calculated according to the error propagation method).

Table 4
Comparison of main product yields with studies from literature.

		This study	This study	Jung et al. [21]	Kaminsky [22]	Kaminsky [22]	Mandviwala et al. [31]
Feedstock	–	PP	PE	PP	PE	PP	PE
Fluidization medium	–	Steam + N_2	Steam + N_2	Product gas	Product gas	Product gas	Steam
Temperature	°C	742	744	746	750	750	750
Residence time	s	1.6 – 8.2	1.8 – 9.7	N/A	N/A	N/A	N/A
Non-condensable product gas	m/m%	55 – 58	61—67	67	74	52	83
Benzene + toluene	m/m%	14—22	14 – 19	14	16	25	12
Aromatics	m/m%	7.2—14	6.6—11	12	7.4	12	7.4
Solid carbon	m/m%	1.9	2.1	4.0	0.9	1.6	0.9

while the yields of aromatics and solid carbon were lower, which can be attributed to shorter residence times in their reactor.

For all three feedstocks, the yields of the non-condensable gas decreased with increasing gas phase residence time (A–C), while the yields of the condensable products namely benzene + toluene and tar increased. For DKR-350, the mass yield of the non-condensable product gas decreased by 7.0 m/m%. This mass was re-distributed between the benzene + toluene, which showed a 5.1 m/m/% increase in mass yield and the tar which increased by 3.7 m/m% (note the difference between the total mass balance closure between point A and C was 1.9 m/m%). The results indicate that with increasing residence time, a greater fraction of the non-condensable gas mass was converted into benzene and toluene, and a smaller fraction into other aromatics. For PE, the non-condensable product gas decreased with 6 m/m% (from point A–C). This mass was redistributed between benzene + toluene and tar, which increased by 4.6 and 4.8 m/m% respectively (note the difference between the total mass balance closure between point A and C was 3.8 m/m%).

As the gas phase residence time in the reactor increased, the primary products formed during thermal cracking underwent secondary reactions to form more complex and larger molecules [21,32]. For example, C_3H_6 was formed during the primary cracking reactions of PP, but underwent secondary reactions to form benzene, toluene and larger PAHs via hydrogen abstraction, carbon addition mechanism [9]. The non-condensable product gas yields for PE and DKR-350 were higher compared to that of PP (specifically comparing position B and C), with the yields ranging between 63–70 m/m% for the PE and DKR-350 and between 55–58 m/m% for PP. Conversely the yields of benzene + toluene (21–22 m/m%) and tar (14 m/m%) were higher for PP, compared to PE and DKR-350 which had 17–19 m/m%, benzene + toluene yields and 11–12 m/m % for the tar yields. This suggests that for PP more secondary reactions occurred in the gas phase, leading to higher yields of secondary products such as benzene, toluene and tar components (refer to Section 3.2 and 3.3 for a more detailed discussion). Lastly, the combusted material yields (solids) reported were the same for all residence times, as it is based on the residual carbon in the bed and not soot formed during secondary reactions. The secondary reactions can lead to the formation of soot (solid carbon), however for this study the solid carbon was not measured at each point as the solids mainly remained in the bed and the soot was filtered out in the pre-sampling system of the gas analysis (see Section 2.3). The amount of the soot in the filter was negligible and could not be reliably quantified.

3.2. Non-condensable gases

In Figs. 3 to 5, the yields of the non-condensable gases are compared for PE, PP and DKR-350.

For all three feedstocks, the primary products in the non-condensable product gas phase were CH_4, C_2H_4 and H_2, with the C_3H_6 present in lower yields. Green & Sadrameli [33] studied the thermal degradation of PE under pyrolysis conditions, which showed that for temperatures ≥ 750 °C CH_4 + C_2H_4 have the highest yields (mass based), followed by aromatics, Other studies have also indicated that C_2H_4 is a dominant component in the product gas along with CH_4 for the thermal

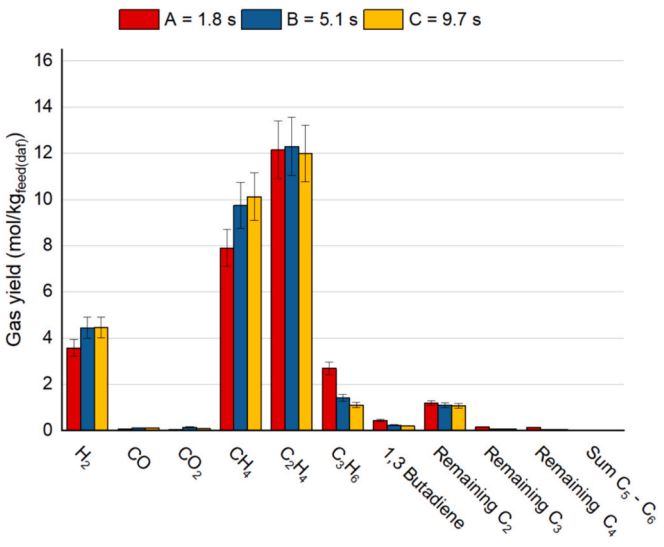

Fig. 3. Comparison of non-condensable gas component yields for PE at 750 °C for different residence times (Error bars calculated according to error propagation method).

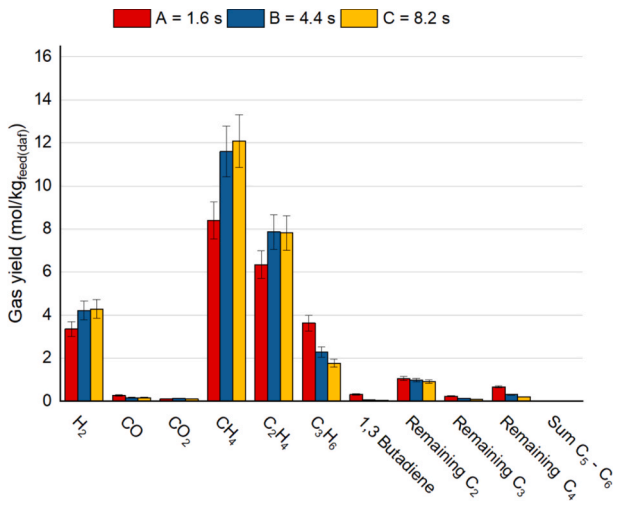

Fig. 4. Comparison of non-condensable gas component yields for PP at 750 °C for different residence times (Error bars calculated according to error propagation method).

degradation of PE [21–24,32]. The C_2H_4 monomer is produced by chain-end β-scission reactions, while C_3H_6 and butene (C_4H_8) are formed via intra-molecular hydrogen transfer reactions. The rate of chain-end β-scission reactions show a larger extent at higher temperatures compared to intra-molecular hydrogen transfer and for this reason the C_2H_4 is significantly higher than the C_3H_6 and C_4H_8 yields [24,34].

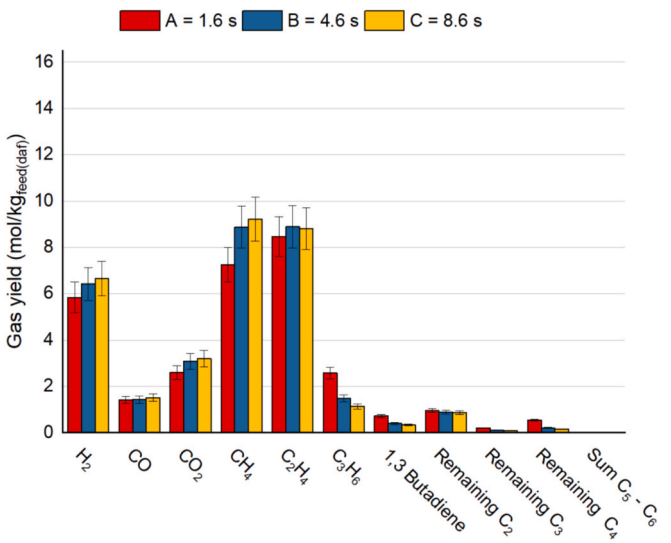

Fig. 5. Comparison of non-condensable gas component yields for DKR-350 at 750 °C for different residence times (Error bars calculated according to error propagation method).

For PP, the yields of C_3H_6 and CH_4 increased and conversely the yield of C_2H_4 decreased compared to PE, while the H_2 yield remained comparable, which is in line with the results reported by Wilk & Hofbauer [35]. Abbas-Abadi [36] reported that the additional methyl group in the polymer backbone of PP reduces its thermal stability compared to PE. The structural difference facilitates quicker thermal degradation of PP, where random chain scission becomes the dominant pathway. Jung et al. [21] further explained that C_3H_6 is more readily formed during PP pyrolysis due to random scission producing primary and secondary radicals, followed by intramolecular radical-transfer reactions, leading to the formation of tertiary radicals. Subsequent β-cleavage of the tertiary radicals promotes the formation of C_3H_6. As a result, the C_3H_6 yield is higher, as also reported by other studies [21–23]. The gas phase product yields of DKR-350 (which contained 68 % PP-PE fraction) were comparable with the yields of pure PE and PP respectively. C_2H_4 and CH_4 had the highest yields, with the C_3H_6 yield being lower and comparable with yield for PE. The H_2 yield was higher compared to the pure polymers, as well as the CO and CO_2 yields. The CO and CO_2 yields were higher due to the presence of oxygen containing polymers such as PET and biogenic material (e.g. food and paper) in the DKR-350 waste.

During thermal decomposition/cracking, polymer chains of PP and PE undergo random scission of the carbon–carbon (C–C), initiating primary cracking reactions through the release of free radicals. These free radicals propagate degradation through further C–C bond cleavage and carbon-hydrogen (C–H) bond cleavage (hydrogen abstraction), thereby generating additional radicals. The resulting radical species subsequently react to form smaller hydrocarbons (e.g. CH_4, C_2H_4 and C_3H_6) and H_2, which constitutes the primary products of PE and/or PP thermal cracking [9,17,18,23,36]. As temperature and residence time increase, these primary products undergo secondary reactions in the gas phase to form secondary products, namely aromatics (benzene and toluene), syngas (CO and H_2), CO_2, CH_4 and solid carbon (soot) [9,17,24]. Aromatics are formed via Diels-Alder reactions and dehydrogenation reactions, where H_2 is produced as a co-product [18,21,24,37]. Syngas is formed during steam reforming, where steam reacts with hydrocarbons to form CO and H_2. CO_2, in turn, is formed during the water–gas-shift (WGS) reaction, where the produced CO is consumed together with steam to yield CO_2 and H_2. CH_4 is formed during the primary cracking reactions, but the concentration continues to increase with the occurrence of secondary reactions, namely further cracking of the larger hydrocarbons and reactions such as radical recombination and hydrogen abstraction [18,20,37,38].

The occurrence of secondary reactions with increasing gas phase residence time was evident from the increase in H_2 and CH_4 yields and subsequent decrease in the yields of C_3H_6 and larger hydrocarbons (C_3+). The most significant effect of gas phase residence time was seen for the initial step going from point A to B, where the largest decrease in primary product yields (C_3H_6 and butadiene) and largest increase in the secondary product (CH_4 and H_2) yields were seen. For PE, the C_3H_6 yield decreased with 47 %, while for PP the yield decreased with 37 %. The CH_4 and H_2 increased with 23 and 24 % respectively for the PE feedstock and with 38 and 26 % respectively for the PP feedstock. For the second step (going from point B to C), a further decrease in C_3H_6 and butadiene was seen, but the change in yield was less significant compared to the initial step. For example, for the PE feedstock the C_3H_6 yields decreased with 22 % from point B to C. Conversely, the H_2 and CH_4 yields increased with 4 % and 0.3 % respectively from point B to C (falls withing the error margin). Thus, in the second step the decrease in C_3H_6 yield does not contribute to further increase in the CH_4 and H_2 yield, but instead to the formation of other secondary products such as benzene (discussed in Section 3.3).

For the C_2H_4 yields, it is seen that for PE the yields remained constant for all residence times, indicating that C_2H_4 was not significantly influenced by gas phase residence time. For PP, the C_2H_4 yield increased with 24 % going from point A to B and proceeded to remain constant from point B to C. Comparing the PP and PE yields, it is seen that the remaining C_4 hydrocarbon yield was higher for the PP feedstock, due to higher concentrations of *iso*-C_4H_8 in the product gas. As the residence time increased, C_4H_8 underwent secondary cracking reactions contributing to the increase in C_2H_4 yield with residence time. In the study of Gholami et al. [18] a trend can be seen between the C_2H_4 and C_4H_8 yields under different conditions, where the C_4H_8 decreased and C_2H_4 yield subsequently increased. Green & Sadrameli [33] reported that during pyrolysis (under N_2) of PE, the CH_4 and C_2H_4 yields increased with residence time, though the rate of increase declines for higher temperatures. Conversely, the C_4 hydrocarbon yields initially rise but proceed to decline, with higher temperatures accelerating the decline with residence times. Westerhout et al. [23] stated that products of PP pyrolysis namely C_3H_6 and C_4H_8 were more reactive compared to C_2H_4 which was the main product of PE pyrolysis. They observed an increase in C_2H_4 yields, which coincided with the decrease in C_3H_6 and C_4H_8 yields and suggested that the C_2H_4 formation may result from the decomposition of C_3H_6 and C_4H_8. Similar trends for C_2H_4, C_3H_6 and C_4H_8 yields were also reported for steam cracking of PE under various temperatures and was attributed to secondary reactions of C_3H_6 and C_4H_8 [24]. Fu et al. [34] showed a continuous increase in C_2H_4 yields with residence time, while the C_3H_6 and C_4H_8 yields started to decline for a residence time > 0.4 s.

In general, the trends of the yields were comparable for all three feedstocks. The largest change in yields was seen for the first step going from point A to B (gas phase residence time of circa 3 s difference), suggesting that the gas phase the residence time effect becomes less pronounced as the time increases. The largest decrease in primary product yield was seen for C_3H_6 compared to C_2H_4 and larger hydrocarbons for which the yields were already marginal. This indicates that C_3H_6 was more reactive (compared to C_2H_4) and readily undergoes secondary reactions to form aromatics (see Section 3.3 for further details), CH_4 and H_2. Previous studies investigating the effect of temperature and residence time on the product distribution have shown that the C_3H_6 yield tends to decreases more readily compared to C_2H_4 under conditions promoting secondary reactions, suggesting a higher reactivity of C_3H_6 [9,18,21–23,39]. Gholami et al. [18] reviewed the effect of residence time on the hydrocarbon product distribution during steam cracking, with the results showing a general downwards trend for C_3H_6 yield with residence time and increased yield of CH_4, H_2 and aromatics (e.g. benzene). Park et al. [38] showed that for pyrolysis of PP (under N_2 atmosphere) in a fluidized bed, longer residence times led to increased yields of H_2, CH_4 and aromatics. The yields of C_3H_6, C_2H_4 and larger

hydrocarbons decreased, with the biggest decrease seen for C_3H_6. The presence of the methyl group in C_3H_6 reduces the thermal stability (similar to PP), facilitating easier formation of radicals and higher reactivity. Specifically, the bond dissociation energy of the allylic C–H bond is lowered, facilitating the formation of resonance-stabilized allyl radicals via β-scission and hydrogen abstraction, which in turn promotes secondary radical reactions and cyclization (via recombination). A more detailed explanation into the mechanism can be found in [9,20,40].

Apart from CH_4 and H_2, CO and CO_2 are secondary products produced during steam reforming of hydrocarbons (forms H_2 and CO) and the WGS reaction (forms H_2 and CO_2). For PE, the yields of CO and CO_2 were negligibly small (< 0.15 mol/$kg_{feed(daf)}$), indicating that steam reforming and WGS were not the main secondary reactions responsible for H_2 formation [24]. For PP, a small CO yield was observed at point A (0.27 mol/$kg_{feed(daf)}$), which could be due to limited steam reforming activity either with residual solid carbon or hydrocarbons. As the residence time increased, the CO yield decreased to 0.17 mol/$kg_{feed\ (daf)}$ which could be due to some consumption in WGS to form H_2 and CO_2, however the CO_2 yield was minimal (0.15 mol/$kg_{feed(daf)}$), indicating a limited role of WGS. Steam reforming reactions are endothermic (favouring higher temperatures) and the operating conditions for this study were likely not suitable for the reaction to have a significant effect on the product distribution. Li et al. [41] investigated steam cracking of PET under similar temperatures and indicated that the effect of steam reforming and WGS reactions would be minimal.

For the DKR-350 feedstock, the yields of CO and CO_2 were higher due to the presence of oxygen in the feedstock (see Table 1). The H_2 yield gradually increased with residence time, while the CO yield remained constant. The CO_2 yield increased which could be attributed to the limited extent of the WGS reaction as well as further thermal degradation of PET, which leads to the release of CO_2 [41].

3.3. Aromatics

The yields of benzene and toluene are presented in Figs. 6 to 8, together with the yields of the different tar classes for the three different feedstocks. The PAH components were grouped together according to the tar classification system defined by Van Paasen & Kiel [42]. In the SI (Table S4) the yields of the individual components are reported for each feedstock.

For all three feedstocks, benzene had the highest yield of all the measured aromatics, followed by toluene and the class 4 tar (light PAH compounds; 2 & 3 ring) at longer residence times. The benzene yields for both the PE and DKR-350 feedstock were comparable, exhibiting a similar yield trend increase with the gas phase residence time. Specifically, from point A to B, the benzene yield increased with 29 % for both feedstocks. From point B to C, the benzene yield increased with 6 % for PE and 10 % for DKR-350. These trends correlate with the C_3H_6 behaviour in the gas phase, where similar initial yields and subsequent decreases were seen for both feedstocks. From point A to B the C_3H_6 yield decreased with 43–47 % and subsequently with 22–23 % from point B to C. The parallel behaviour between DKR-350 and PE aligns with the DKR-350 having a higher PE content compared to PP (see Section 2.1).

For PP, the initial benzene yield (95 g/$kg_{feed(daf)}$) was lower compared to PE and DKR-350 (107—116 g/$kg_{feed\ (daf)}$), however from point A to B the benzene yield increased significantly with 63 %, surpassing the yields of PE and DKR-350. The significant increase in benzene yield correlates once more with the decrease in the C_3H_6 yield in the gas phase. PP had the highest C_3H_6 yield, which decreased with 37 %

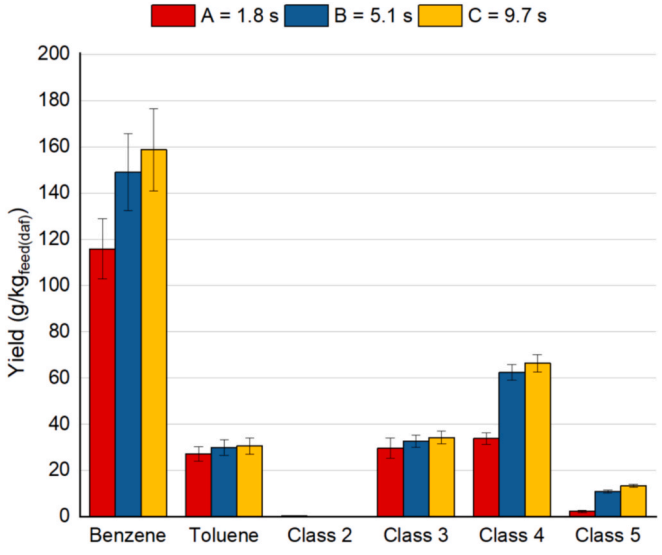

Fig. 6. Comparison of benzene, toluene and tar class yields for PE at 750 °C for different gas phase residence times (Error bars calculated according to error propagation method).

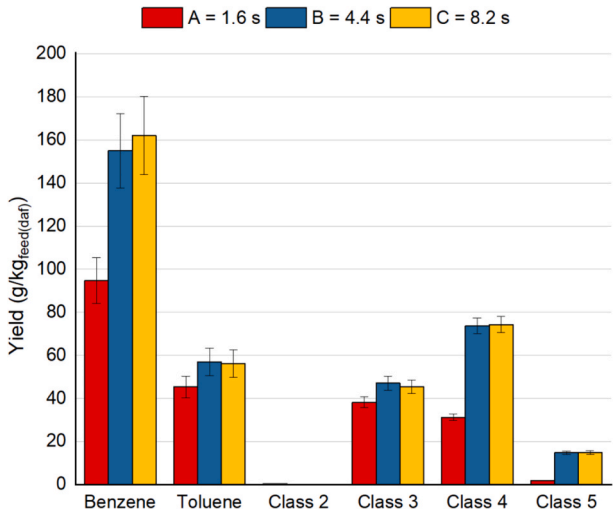

Fig. 7. Comparison of benzene, toluene and tar classes concentration for PP at 750 °C for different gas phase residence times (Error bars calculated according to error propagation method).

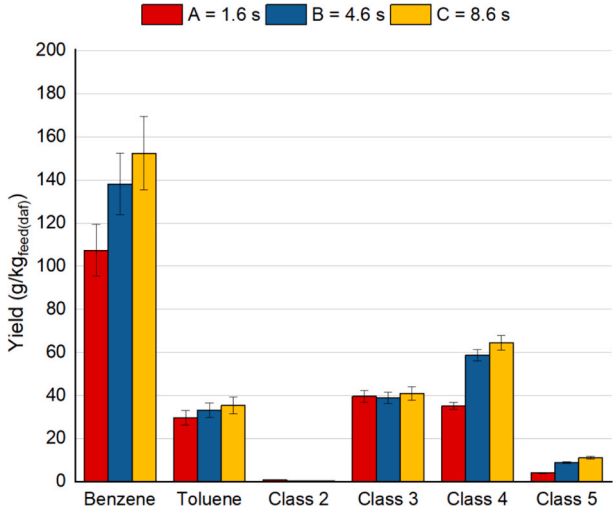

Fig. 8. Comparison of benzene, toluene and tar classes concentration for DKR-350 at 750 °C for different gas phase residence times (Error bars calculated according to error propagation method).

from point A to B, while for PE and DKR-350 the decrease was 42–47 %. On an absolute basis the decrease in C_3H_6 yield for PP was greater (57 g/$kg_{feed\ (daf)}$) compared to PE (54 g/$kg_{feed\ (daf)}$) and DKR-350 (46 g/$kg_{feed\ (daf)}$). The inverse correlation seen for C_3H_6 reduction and benzene formation is consistent across all three feedstocks, indicating that C_3H_6 undergoes secondary reactions to form benzene. Jung et al. [21] and Kaminsky et al. [22] compared the pyrolysis of PE and PP (under similar conditions as for this study) and reported higher yields of benzene and aromatics for PP compared to PE. Jung et al. [21] explained that the higher benzene and aromatics yield for PP was due to a higher concentration of C_3H_6 in the product gas, which more readily takes part in the Diels-Alder reaction to form benzene. As stated in Section 3.2, C_3H_6 readily forms allyl radicals (via β-scission and hydrogen abstraction), which in turn undergo intramolecular or intermolecular cyclization reactions to form cyclic intermediates. The Diels-Alder reaction is one pathway for cyclization reactions, leading to the formation of aromatic rings such as benzene. Subsequent dehydrogenation forms stabilized aromatics [9]. In the SI a simple kinetic scheme summarizing the three main steps from C_3H_6 to C_6H_6 is proposed, for more detailed and complete reaction schemes refer to [9,18,20,40].

Apart from benzene, the yields of the other aromatics also increased with gas phase residence time. For PP, the toluene yield increased which also follows a similar mechanism as for benzene, explaining why the yield also increases [21]. For PP and PE, the class 3 tar, namely the 1-ring aromatics such as xylene and styrene, increased with the residence time. Styrene is formed via Diels-Alder reaction and dehydrogenation of 1,3 butadiene [37]. For DKR-350, the increase was less significant as the feedstock already contains polymers such as PS, which thermally decomposes to produce styrene [9,43,44]. The styrene yield is thus the result of the primary decomposition reaction of PS and to a lesser extent the result of secondary reactions. The class 4 tar, which consists of 2 & 3 ring compounds such as naphthalene, fluorene and biphenyl, increased significantly for all three feedstocks going from point A to B, after which it remained constant. The yield of the class 5 tar (4–7 ring compounds), also increases marginally with residence time for all three feedstocks. Kaminsky & Kim [43] reported that as the residence time increases the tar yield would increase, with higher condensed aromatics being formed in favour of the benzene yield. The formation of larger PAHs via secondary reactions during pyrolysis and steam cracking of polyolefin waste has been reported by numerous studies. However, these studies mostly focused on the effect of higher temperatures facilitating the secondary reactions rather than longer residence time [21,22,24,32,45].

Zhou et al. [46] investigated the formation of PAH from pyrolysis of various municipal solids waste fractions including PE. It was reported that PAHs from PE were mainly formed via Diels-Alder type reactions, where alkenes and dialkenes react to form benzenes. The higher molecular weight PAHs are subsequently formed from the lighter, single-ring compounds (benzene, toluene and styrene) via hydrogen abstraction, acetylene addition or through interactions of naphthalene and cyclopentadiene, or indene and cyclopentadiene. A more detailed explanation of the mechanism can be found in [46]. Naphthalene was reported as the most abundant PAH from PE pyrolysis and was also the main contributor of the class 4 tar yield of all three feedstocks in this study (see Table S4). The change in aromatics concentration was also visually seen from the change in colour of the impingers bottles used to sample aromatics during the tar guideline protocol (see Section 2.3). The photos of the guideline bottle for PP at 750 °C are shown in Fig. 9.

In the SI, the photos for PE and DKR-350 at 750 °C can also be found. The most significant colour change was seen between position A and B, where the colour went from light yellow–brown to a darker orange-brown colour. As the gas phase residence time increased, the lighter PAHs (lower molecular weight) reacted further to produce heavier PAHs (higher molecular weight) resulting in a darker colour. The colour change was especially evident for the first two impingers, where the heavier tar components (higher boiling point) were captured. From point B to C the colour change was not as significant, as it was for the first point. For the second impinger the colour becomes darker, while for the fourth impinger (where the lighter aromatics such as benzene are captured) the concentration also becomes darker, once more indicating the formation of heavier components from the lighter components. The results for PE and DKR-350 were similar and correspond with the changes in concentrations shown in Figs. 6–8.

3.4. Cracking severity

Cracking severity is a measure from steam cracking of hydrocarbons to indicate how many feed molecules are consumed and broken down ('cracked') to smaller molecules [19,20,47]. For this work, the cracking severity coefficient proposed by Mandviwala et al. [31] was used to indicatively compare the cracking severity of different feedstocks for the different gas phase residence times. The index was originally developed for steam cracking of pure high density PE in a fluidized bed. Applying the index to heterogeneous feedstocks introduces limitations due to composition variability, which affects the yields of the products. The calculation is based on the moles of light olefins generated per mole of CH_4 produced, as shown in Eq. (5) in Section 2.4. The index is thus sensitive to CH_4 yield accuracy, with large errors in the CH_4 quantification leading to an over- or underestimation of the cracking severity. For this study the errors in CH_4 yields were comparable, as seen in Section 3.2. The cracking severity coefficients for the different residence times and feedstocks are presented in Fig. 10. The cracking severity coefficient was also calculated for the experiment with PE at 700 °C (see run 4, Table 2) and is also presented in Fig. 10. A higher cracking severity coefficient corresponds to a lower cracking severity, as it is inversely proportional to the methane production.

The cracking severity increased with residence time for all runs, corresponding with the results in Section 3.2. The decrease in C_3H_6 yield and corresponding increase in CH_4 yield were the primary contributors to the decrease in the cracking severity coefficient. The C_2H_4 yield remained mostly constant and the C_4H_8 yields were initially low and did not contribute significantly to the cracking severity coefficients. For the experimental runs at 750 °C, all cracking severity coefficients were below two. For steam cracking of PE at 750 °C in a laboratory-scale fluidized bed reactor, Mandviwala et al. [31] reported a cracking severity coefficient of 1.93 which is in-line with the PE cracking for this

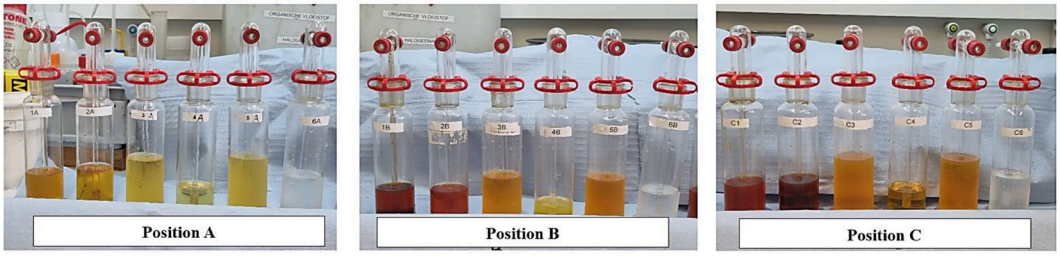

Fig. 9. Photos of tar guideline impinger bottles for PP at 750 °C at difference positions (and residence times).

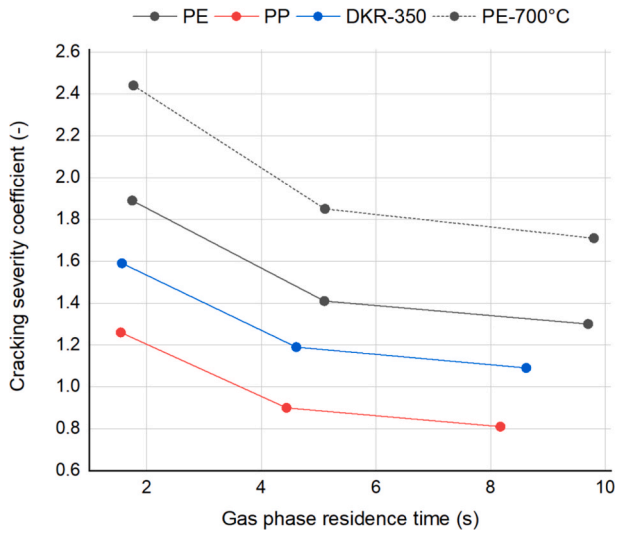

Fig. 10. Comparison of cracking severity coefficient as function of gas phase residence time for different feedstocks and temperatures.

study, namely 1.89 at the initial gas phase residence time point. Comparison of the feedstocks showed that PP had the highest reactivity by having the highest cracking severity. This is attributed to PP being more reactive compared to PE and also having higher C_3H_6 yields, which in turn was more reactive compared to C_2H_4 (main product for PE). The cracking severity coefficient of DKR-350 fell between that of PE and PP, which is in line with the waste containing 68 % PE-PP. Looking at the trend the biggest decrease in cracking severity coefficient was seen for the first step in residence time, with the coefficient decreasing with 25–29 % for all feedstocks. For the second step the decrease in cracking severity coefficient was 8–10 % for all feedstocks. The trend in cracking severity corresponds with the trend seen for the gas components yields in Section 3.2, where the largest decrease in primary products (mainly C_3H_6) and corresponding largest increase in secondary products (mainly CH_4 and H_2) were seen going from point A to B. The fluidized bed was the primary reactive zone, where extensive radical formation occurs, due to the initial scission of polymer chains, which subsequently leads to the generation of primary products. At a gas phase residence time of ± 2 s above the fluidized bed (the top of the bed was taken as the baseline for 0 s – see Section 2.3), there is still a significant amount of free radicals which promote secondary cracking reactions, leading to the formation of secondary products. In the SI (Fig. S10) the collective carbon yields of light olefins (C_2H_4, C_3H_6 and 1,3 butadiene) are compared with the carbon yields of CH_4, benzene + toluene and the tar components. Most of the carbon mass of the light olefins went towards the production of benzene + toluene. For a gas phase residence time above five seconds (B–C) the free radical concentration decreases, resulting in a lower extent of secondary reactions and a smaller increase in the yield of secondary products.

The cracking severity coefficient was higher for a lower temperature, as cracking was less severe at lower temperatures. For PE at the initial gas phase residence time, the cracking severity coefficient was 2.44 at 700 °C. With the increase in temperature the coefficient decreased with 23 %, similar to the decrease in the initial step in gas phase residence time for PE at 750 °C. Temperature and residence time are both parameters that promote secondary reactions during thermal cracking of hydrocarbons. Westerhout et al. [23] investigated the effect of residence time ranging from 0.1 to 1 s (temperature 650 – 800 °C) on the pyrolysis of PE and PP, with the conclusion that residence time had a minimal effect when compared to temperature for the given experimental conditions. The results showed minimal increase in the CH_4 and C_2H_4 yield with residence time, while the C_3H_6 yield remained constant. Van Greem et al. [20] noted that for steam crackers the residence time is not an independent variable, but linked to the temperature profiles in the reactors. For steam crackers the severity parameter used to calculate the cracking severity is usually a combination of temperature and residence time [19].

4. Conclusions

The effect of gas phase residence time on the thermal cracking product slate of polyolefin-rich waste was experimentally investigated. Varying residence times were investigated by simultaneously sampling the product gas at three different positions above the bed, which allowed for a direct comparison of the gas phase residence time effect. For all three feedstocks, the non-condensable gas yield decreased with gas phase residence time in favour of condensable secondary products namely benzene and toluene, as well as tar components. The increased yields were due to longer residence times promoting secondary reactions such Diels-Alder and dehydrogenation, which lead to the formation of aromatics. For the gas phase yields, C_3H_6 was the most reactive primary product, reacting to form secondary products namely CH_4 and H_2. The C_2H_4 was more stable and the yield mostly remained constant. For PP, the C_2H_4 yield increased due to the thermal decomposition of C_3H_6 and C_4H_8.

Benzene had the highest yield of the aromatics, increasing with residence time due to secondary aromatization reactions. For longer residence times, the heavier aromatics yields also increased. The cracking severity coefficient indicated that the cracking severity increased with residence time, with PP showing the highest cracking severity and PE the lowest due to its greater thermal stability. At lower temperatures, the cracking was less severe due to secondary reactions being promoted at higher temperatures. The largest impact of gas phase residence time was seen for the first step namely 1.6 to 5 s, with the second time step seeing a lesser effect, which was attributed to the concentration of free radicals in the different zones. At a gas phase residence time of 1.6 s above the fluidized bed, free radicals are still present in significant amounts promoting secondary reactions. For a gas phase residence time above 5 s, the free radical concentration decreases, leading to a decrease in the extent of secondary reactions. Comparison of the product distribution for the three feedstocks showed that DKR-350 had a product slate more consistent with pure PE than PP and exhibited similar trends with gas phase residence time. The cracking severity coefficient and product distribution for DKR-350 could thus be predicted based on the behaviour of pure PE, as PE had the highest fraction in the feedstock.

The results of this study provide insight into the role of gas phase residence time on the formation of secondary products during the thermal cracking of the polyolefin-rich waste. The results can support reactor design and operation for industrial plastic waste processing, depending on the desired product slate. For light olefin production short residence times are favoured (< 1.6 s), which are achievable through higher flow rates, smaller reactor volumes or quenching and dilution to suppress secondary reactions. In contrast, for BTXS production slightly longer residence times (1.6 – 5 s) are favoured, though too long residence times can lead to the formation of larger PAHs and soot. These findings aid process optimization, by guiding process conditions to maximize product yields, while minimizing reactor fouling and emissions.

CRediT authorship contribution statement

Surika van Wyk: Writing – original draft, Visualization, Investigation, Methodology, Validation, Data curation, Formal analysis, Conceptualization. **Carlos F. Mourao Vilela:** Writing – review & editing, Project administration, Methodology, Funding acquisition, Conceptualization. **Carel Meijwes:** Resources, Methodology, Investigation. **Marco Geusebroek:** Methodology, Investigation, Data curation. **Arnold Toonen:** Methodology, Investigation, Data curation.

Declaration of competing interest

The authors declare that they have no known competing financial interests or personal relationships that could have appeared to influence the work reported in this paper.

Acknowledgements

SYNOVA and the Dutch Ministry of Economic Affairs and Climate Policy for subsidizing this work within the GRIP project with the number Chemie.PGT.2024.043. The authors would also like to thank Pedro Abelha, Sander Grootjes, Robin Zwart and Bram van der Drift for reviewing the paper prior to submission.

Appendix A. Supplementary material

Supplementary data to this article can be found online at https://doi.org/10.1016/j.fuel.2025.137561.

Data availability

Data will be made available on request.

References

[1] Dokl M, Copot A, Krajnc D, Fan YV, Vujanović A, Aviso KB, et al. Global projections of plastic use, end-of-life fate and potential changes in consumption, reduction, recycling and replacement with bioplastics to 2050. Sustain Prod Consum 2024;51:498–518. https://doi.org/10.1016/j.spc.2024.09.025.
[2] Oecd. Global plastics outlook: economic drivers, environmental impacts and policy options. OECD 2022. https://doi.org/10.1787/de747aef-en.
[3] Schulze-Netzer C. Gasification for material recycling—a solution to the plastic flood? Can J Chem Eng 2024;102:2966–79. https://doi.org/10.1002/cjce.25301.
[4] Malin Castell Rudenhausen, Anna Tenhunen-Lunkka, Alesso d'Amato, Alexandra Almasi, Ive Vanderreydt, Lars Fogh Mortensen, Tobias Nielsen. ETC CE Report 2024/6 Measuring Europe's plastics circularity - through the lenses of the EEA Circularity Metrics Lab. uropean Environment Information and Observation Network; 2024.
[5] Kibria MG, Masuk NI, Safayet R, Nguyen HQ, Mourshed M. Plastic waste: challenges and opportunities to mitigate pollution and effective management. Int J Environ Res 2023;17:20. https://doi.org/10.1007/s41742-023-00507-z.
[6] Plastics Europe. Plastics - the fast Facts 2024. Plastics Europe; 2024.
[7] Thunman H, Berdugo Vilches T, Seemann M, Maric J, Vela IC, Pissot S, et al. Circular use of plastics-transformation of existing petrochemical clusters into thermochemical recycling plants with 100% plastics recovery. Sustain Mater Technol 2019;22:e00124. https://doi.org/10.1016/j.susmat.2019.e00124.
[8] Lange J-P, Kersten SRA, Meester SD, Ragaert K. Plastic recycling stripped naked – from circular product to circular industry with recycling cascade 2024.
[9] Dogu O, Pelucchi M, Van De Vijver R, Van Steenberge PHM, D'hooge DR, Cuoci A, et al. The chemistry of chemical recycling of solid plastic waste via pyrolysis and gasification: state-of-the-art, challenges, and future directions. Prog Energy Combust Sci 2021;84:100901. https://doi.org/10.1016/j.pecs.2020.100901.
[10] Plastics Europe. The Circular Economy for Plastics - A European Analysis. Plastics Europe; 2024.
[11] Lopez G, Artetxe M, Amutio M, Bilbao J, Olazar M. Thermochemical routes for the valorization of waste polyolefinic plastics to produce fuels and chemicals. a review. Renew Sustain Energy Rev 2017;73:346–68. https://doi.org/10.1016/j.rser.2017.01.142.
[12] Zhao X, Korey M, Li K, Copenhaver K, Tekinalp H, Celik S, et al. Plastic waste upcycling toward a circular economy. Chem Eng J 2022;428:131928. https://doi.org/10.1016/j.cej.2021.131928.
[13] Mneimneh F, Haddad N, Ramakrishna S. Recycle and reuse to reduce plastic waste - a perspective study comparing petro- and bioplastics. Circ Econ Sustain 2024;4:1983–2010. https://doi.org/10.1007/s43615-024-00381-7.
[14] Lopez G, Artetxe M, Amutio M, Alvarez J, Bilbao J, Olazar M. Recent advances in the gasification of waste plastics. a critical overview. Renew Sustain Energy Rev 2018;82:576–96. https://doi.org/10.1016/j.rser.2017.09.032.
[15] Mandviwala C, Forero Franco R, Berdugo Vilches T, Gogolev I, González-Arias J, Cañete Vela I, et al. Steam cracking in a semi-industrial dual fluidized bed reactor: tackling the challenges in thermochemical recycling of plastic waste. Chem Eng J 2024;500:156892. https://doi.org/10.1016/j.cej.2024.156892.
[16] Krause L, Özgen A, Kern J, Das S, Carus M, Raschka A. Mapping of advanced plastic waste recycling technologies and their global capacities. Nova-Institut GmbH 2024. https://doi.org/10.52548/WQHT8696.
[17] Forero-Franco R, Cañete-Vela I, Berdugo-Vilches T, González-Arias J, Maric J, Thunman H, et al. Correlations between product distribution and feedstock composition in thermal cracking processes for mixed plastic waste. Fuel 2023;341:127660. https://doi.org/10.1016/j.fuel.2023.127660.
[18] Gholami Z, Gholami F, Tišler Z, Vakili M. A review on the production of light olefins using steam cracking of hydrocarbons. Energies 2021;14:8190. https://doi.org/10.3390/en14238190.
[19] Golombok M, Van Der Bijl J, Kornegoor M. Severity parameters for steam cracking. Ind Eng Chem Res 2001;40:470–2. https://doi.org/10.1021/ie990436r.
[20] Van Geem KM, Reyniers M-F, Marin GB. Two severity indices for scale-up of steam cracking coils. Ind Eng Chem Res 2005;44:3402–11. https://doi.org/10.1021/ie048988j.
[21] Jung S-H, Cho M-H, Kang B-S, Kim J-S. Pyrolysis of a fraction of waste polypropylene and polyethylene for the recovery of BTX aromatics using a fluidized bed reactor. Fuel Process Technol 2010;91:277–84. https://doi.org/10.1016/j.fuproc.2009.10.009.
[22] Kaminsky W. Chemical recycling of plastics by fluidized bed pyrolysis. Fuel Commun 2021;8:100023. https://doi.org/10.1016/j.jfueco.2021.100023.
[23] Westerhout RWJ, Kuipers JAM, Van Swaaij WPM. Experimental determination of the yield of pyrolysis products of polyethene and polypropene. influence of reaction conditions. Ind Eng Chem Res 1998;37:841–7. https://doi.org/10.1021/ie970384a.
[24] Mollick M, Santamaria L, Cortazar M, Mollick PK, Comendador P, Amutio M, et al. Evaluation of temperature role in the HDPE steam cracking product distribution with a focus on light olefins production. J Anal Appl Pyrol 2025;186:106922. https://doi.org/10.1016/j.jaap.2024.106922.
[25] Natesakhawat S, Weidman J, Garcia S, Means NC, Wang P. Pyrolysis of high-density polyethylene: degradation behaviors, kinetics, and product characteristics. J Energy Inst 2024;116:101738. https://doi.org/10.1016/j.joei.2024.101738.
[26] Mastral FJ, Esperanza E, García P, Juste M. Pyrolysis of high-density polyethylene in a fluidised bed reactor. influence of the temperature and residence time. J Anal Appl Pyrol 2002;63:1–15. https://doi.org/10.1016/S0165-2370(01)00137-1.
[27] Shah HH, Amin M, Iqbal A, Nadeem I, Kalin M, Soomar AM, et al. A review on gasification and pyrolysis of waste plastics. Front Chem 2023;10:960894. https://doi.org/10.3389/fchem.2022.960894.
[28] Genuino HC, Ruiz MP, Heeres HJ, Kersten SRA. Pyrolysis of mixed plastic waste (DKR-350): effect of washing pre-treatment and fate of chlorine. Fuel Process Technol 2022;233:107304. https://doi.org/10.1016/j.fuproc.2022.107304.
[29] Van de Kamp WL, De Wild PJ, Knoef HAM, Neeft JPA, Kiel JHA. Tar measurement in biomass gasification, standardisation and supporting R&D. TNO (past ECN) 2006.
[30] Aranda Almansa G, Mourao Vilela C, Vreugdenhil BJ. Gas analysis in gasification of biomass and waste guideline report document 1. IEA Bioenergy 2018.
[31] Mandviwala C, González-Arias J, Berdugo Vilches T, Seemann M, Thunman H. Comparing bed materials for fluidized bed steam cracking of high-density polyethylene: olivine, bauxite, silica-sand, and feldspar. J Anal Appl Pyrol 2023;173:106049. https://doi.org/10.1016/j.jaap.2023.106049.
[32] Mastral FJ, Esperanza E, Berrueco C, Juste M, Ceamanos J. Fluidized bed thermal degradation products of HDPE in an inert atmosphere and in air–nitrogen mixtures. J Anal Appl Pyrol 2003;70:1–17. https://doi.org/10.1016/S0165-2370(02)00068-2.
[33] Green AES, Sadrameli SM. Analytical representations of experimental polyethylene pyrolysis yields. J Anal Appl Pyrol 2004;72:329–35. https://doi.org/10.1016/j.jaap.2004.07.006.
[34] Fu Z, Hua F, Yang S, Wang H, Cheng Y. Evolution of light olefins during the pyrolysis of polyethylene in a two-stage process. J Anal Appl Pyrol 2023;169:105877. https://doi.org/10.1016/j.jaap.2023.105877.
[35] Wilk V, Hofbauer H. Conversion of mixed plastic wastes in a dual fluidized bed steam gasifier. Fuel 2013;107:787–99. https://doi.org/10.1016/j.fuel.2013.01.068.
[36] Abbas-Abadi MS. The effect of process and structural parameters on the stability, thermo-mechanical and thermal degradation of polymers with hydrocarbon skeleton containing PE, PP, PS, PVC, NR, PBR and SBR. J Therm Anal Calorim 2021;143:2867–82. https://doi.org/10.1007/s10973-020-09344-0.
[37] Park K-B, Jeong Y-S, Guzelciftci B, Kim J-S. Characteristics of a new type continuous two-stage pyrolysis of waste polyethylene. Energy 2019;166:343–51. https://doi.org/10.1016/j.energy.2018.10.078.
[38] Park K-B, Jeong Y-S, Kim J-S. Activator-assisted pyrolysis of polypropylene. Appl Energy 2019;253:113558. https://doi.org/10.1016/j.apenergy.2019.113558.
[39] Kaminsky W, Predel M, Sadiki A. Feedstock recycling of polymers by pyrolysis in a fluidised bed. Polym Degrad Stab 2004;85:1045–50. https://doi.org/10.1016/j.polymdegradstab.2003.05.002.
[40] Nagaraja SS, Sahu AB, Panigrahy S, Curran HJ. A fundamental study on the pyrolysis of hydrocarbons. Combust Flame 2021;233:111579. https://doi.org/10.1016/j.combustflame.2021.111579.
[41] Li S, Cañete Vela I, Järvinen M, Seemann M. Polyethylene terephthalate (PET) recycling via steam gasification – the effect of operating conditions on gas and tar composition. Waste Manag 2021;130:117–26. https://doi.org/10.1016/j.wasman.2021.05.023.
[42] van Paasen, S.V.B., Kiel, J.H.A. Tar formation in fluidised-bed gasification - Impact of gasifier operating conditions. 2nd World Conf. Technol. Exhib. Biomass Energy Ind. Clim. Prot., Rome, Italy: 2004.
[43] Kaminsky W, Kim J-S. Pyrolysis of mixed plastics into aromatics. J Anal Appl Pyrol 1999;51:127–34. https://doi.org/10.1016/S0165-2370(99)00012-1.
[44] Singh RK, Ruj B, Sadhukhan AK, Gupta P. Impact of fast and slow pyrolysis on the degradation of mixed plastic waste: product yield analysis and their characterization. J Energy Inst 2019;92:1647–57. https://doi.org/10.1016/j.joei.2019.01.009.
[45] Cho M-H, Jung S-H, Kim J-S. Pyrolysis of mixed plastic wastes for the recovery of benzene, toluene, and xylene (BTX) aromatics in a fluidized bed and chlorine

removal by applying various additives. Energy Fuels 2010;24:1389–95. https://doi.org/10.1021/ef901127v.
[46] Zhou H, Wu C, Onwudili JA, Meng A, Zhang Y, Williams PT. Polycyclic aromatic hydrocarbons (PAH) formation from the pyrolysis of different municipal solid waste fractions. Waste Manag 2015;36:136–46. https://doi.org/10.1016/j.wasman.2014.09.014.
[47] Ren T, Patel M, Blok K. Olefins from conventional and heavy feedstocks: energy use in steam cracking and alternative processes. Energy 2006;31:425–51. https://doi.org/10.1016/j.energy.2005.04.001.